

A General Control Method for Human-Robot Integration

Maddalena Feder^{1,2}, Giorgio Grioli^{1,2}, Manuel G. Catalano¹ and Antonio Bicchi^{1,2}

Abstract—This paper introduces a new generalized control method designed for multi-degrees-of-freedom devices to help people with limited motion capabilities in their daily activities. The challenge lies in finding the most adapted strategy for the control interface to effectively map user’s motions in a low-dimensional space to complex robotic assistive devices, such as prostheses, supernumerary limbs, up to remote robotic avatars. The goal is a system which integrates the human and the robotic parts into a unique system, moving so as to reach the targets decided by the human while autonomously reducing the user’s effort and discomfort. We present a framework to control general multi DoFs assistive systems, which translates user-performed compensatory motions into the necessary robot commands for reaching targets while canceling or reducing compensation. The framework extends to prostheses of any number of DoF up to full robotic avatars, regarded here as a sort of “whole-body prosthesis” of the person who sees the robot as an artificial extension of their own body without a physical link but with a sensory-motor integration. We have validated and applied this control strategy through tests encompassing simulated scenarios and real-world trials involving a virtual twin of the robotic parts (prosthesis and robot) and a physical humanoid avatar.

Index Terms—Prosthesis control, Assistive Robotics, Avatar robots, Compensatory Control.

I. INTRODUCTION

ASSISTIVE and rehabilitation devices such as powered wheelchairs, assistive robotic arms, and limb prostheses play a crucial role in assisting individuals with severe motor impairments [1], which require daily assistance due to e.g. spinal cord or brain injuries.

The chosen interfaces, such as joysticks, head arrays, and sip-and-puff, often pose challenges in managing assistive devices [2]. They have an impact on aspects such as timing, accuracy, and transient noise [3]. These interfaces are low dimensional and operate discretely, necessitating users to switch between different areas of the control space. Partially autonomous control can reduce cognitive and physical burden on users [1].

In addition to techniques that exploit Inertial Measurement Unit (IMU) sensors in [4] and brain-machine interfaces (BMIs) in [5] to control assistive devices with high number of Degrees of Freedom (DoFs), another approach involves employing dimensionality reduction techniques, such as Principal Component Analysis (PCA), [5]. Beyond the branch of assistive robotics, these control interfaces find applications also in

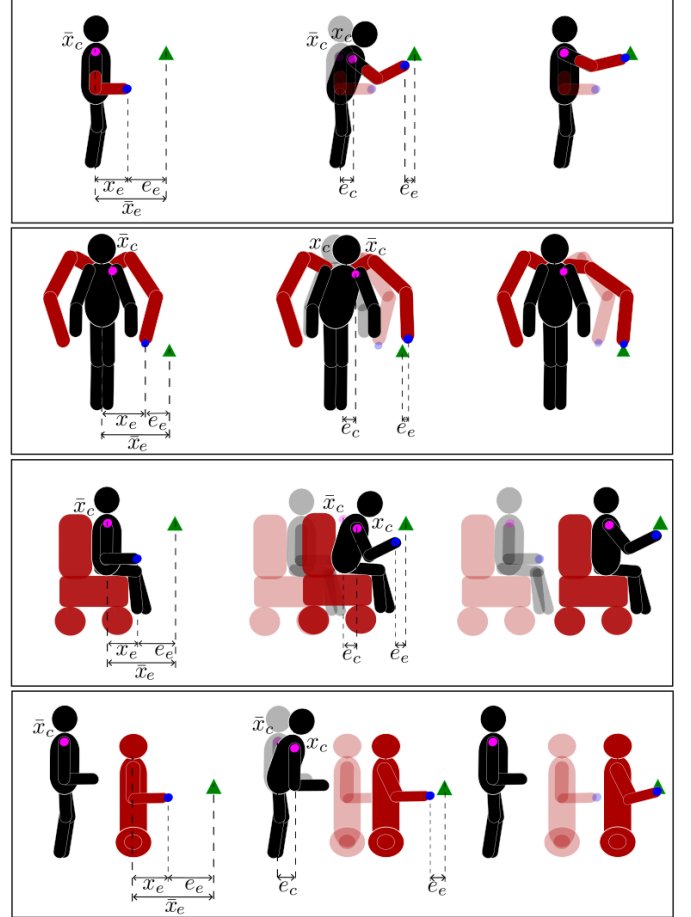


Fig. 1. Starting, intermediate and final phases of the control strategy applied to different assistive robots. Human parts are depicted in black, while artificial parts are in red. Transparency is used to provide a reference to the starting conditions. The green triangle is the target to reach (known only to the human). The blue dot represents the end-effector frame, while the pink dot is the frame where we measure compensation. The rows illustrate applications of our framework to an upper limb prosthesis, to a supernumerary robot limb, to a wheelchair, and to a robot avatar.

human-robot interfaces (HRIs), for both domestic and professional settings. Several studies implement different interfaces to control robotic devices, such as upper-body movements [6], or electromyographic sensors (EMG) on the forearm [7], or sensorised upper-body soft exoskeleton, coupled with virtual reality goggles, [7], or joint-level force control as the ones for the supernumerary robotic limbs [8]. Another interface system, which includes also a haptic admittance module, is presented in [9].

In the prosthetic field, the use of EMG sensors is the most

¹Soft Robotics for Human Cooperation and Rehabilitation, Istituto Italiano di Tecnologia, Genova 16163, Italy (maddalena.feder@iit.it).

²Department of Information Engineering and Centro di Ricerca “Enrico Piaggio”, University of Pisa, 56122, Pisa, Italy.

widely adopted technique [10]. One of the main drawbacks is that as the level of amputation rises, a greater number of sensors is required to provide more inputs, while less independent measurement sites are available. Additionally, a strategy becomes necessary to switch the controller between multiple DoFs. Furthermore, the user's skin condition can impact control performance, as can changes in electrode positions [11]. This control complexity may lead prosthetic users to develop undesired compensatory motion habits, which in turn, can result in postural issues and chronic pain [12].

In recent years, researchers considered that compensatory motions of the patient's body could be themselves useful to control prostheses. [13] used IMUs on the stump in combination with surface EMG signals to control multi-channel prostheses and supernumerary limbs. [14]–[16] more explicitly introduced the idea of exploiting body compensation as a signal to control upper limb prostheses.

Inspired by this work, in this paper we generalize the idea of using compensatory motions in the prosthesis control loop, by including it in a more comprehensive dynamic system view which encompasses both a model of the human user and of the prosthesis and its controller, to be designed.

The generalization of the framework allows us to consistently include widely varying systems, both in the human component, where different abilities can be accommodated for, and in the artificial part, where upper-limb prostheses can be extended to assistive devices and even remote whole-body avatars. Preliminary results in this direction were presented in [17]. In this paper, we substantially extend and improve the framework introducing a model of the human reaching and compensation control, and an observer which can predict the reaching target intention and correct the controlled motion on-line.

We apply this framework to three virtual prosthetic arms with different numbers of joints. We also apply it to the control of a robotic avatar. The avatar, Alter-Ego, is partly human-like, with a torso, head, neck, two arms and hands, but locomotes on two wheels on which it balances. We include the avatar in our control framework by simply regarding it as a prosthesis of the whole body of the user. By this approach, instead of being controlled through classical teleoperation techniques mapping human motions to robot motions one-to-one, the avatar becomes an artificial extension of the human body. In this way, individuals with different motion capabilities are enabled to command the robotic joints through their residual motions as if it were their prostheses.

II. PROBLEM DEFINITION

Consider a dynamic system, composed of a person and a prosthesis of any number of DoFs, up to an artificial replacement of the full body as in an avatar. The system is modelled as a kinematic chain, with n_r robotic joints and n_h human joints. Fig. 1 provides a sketch representation of this model for both a prosthesis, a supernumerary limb, a wheelchair and an avatar. We suppose that the user intent is specified in terms of reaching a desired goal \bar{x}_e with the end

effector x_e , whose position is a function of some or all the n_h human joints q_h and/or the n_r robotic joints q_r as

$$x_e = Q_e(q), \quad (1)$$

where $q = [q_h, q_r]^T$. By defining the human and robotic Jacobian matrices as $J_{he} = J_{he}(q) = \frac{\partial Q_e}{\partial q_h}$ and $J_{re} = J_{re}(q) = \frac{\partial Q_e}{\partial q_r}$, respectively, the differential kinematics of the end effector is

$$\dot{x}_e = [J_{he}(q) \quad J_{re}(q)] \begin{bmatrix} \dot{q}_h \\ \dot{q}_r \end{bmatrix}. \quad (2)$$

We define the reaching error e_e as

$$e_e = \bar{x}_e - x_e. \quad (3)$$

In the following, we assume that the reaching error e_e is known to the user, based on the visual feedback of the displacement between the desired target and their hand. Notice also that both frames are expressed relative to the egocentric reference of the user, which is usually placed in the head. An exception is the avatar case, where the egocentric reference is placed in the head of the avatar itself (through whose eyes the user sees the scene, cf. Fig. 1, last row).

The task for us is to control \dot{q}_r so that e_e tends to zero, and to exploit a possible redundancy in the kinematics of the human-robot system to favor a relaxed configuration of the human joints q_h . The problem is not trivial because the desired final position \bar{x}_e is not available to the robot controller. To circumvent this problem, we exploit the ability of humans to include in their body schema devices and appendages [18], and to exploit them to reach their goals. For example, a person wearing even a completely passive prosthesis, such as a “cosmetic hand”, can easily reach for an object, although at the cost of possibly exaggerated motions of the intact body joints in the shoulder, torso, waist and legs.

Consider hence the case that the user attempts to reach the goal without counting on the assistance of an active prosthesis, as they would do with a passive appendage of some form: the user will employ their own DoFs (q_h) while assuming that the prosthetic joints are fixed ($\dot{q}_r = 0$) in the present configuration. The resulting body motions (which are somehow not natural and possibly fatiguing for the user) are commonly referred to as *compensatory movements*. The idea of exploiting compensatory motions in prosthesis control was first introduced by [16]. Let x_c denote a compensatory reference frame fixed on a selected body segment (e.g. at the shoulder), let \bar{x}_c indicate its posture in a relaxed body posture, and define a compensation error $e_c = \bar{x}_c - x_c$.

In general, also the compensatory frame moves as a function of both the human and robotic joints as

$$x_c = Q_c(q). \quad (4)$$

Let $J_{hc} = J_{hc}(q) = \frac{\partial Q_c}{\partial q_h}$ and $J_{rc} = J_{rc}(q) = \frac{\partial Q_c}{\partial q_r}$ be the Jacobian matrices of the compensatory model with respect to the human and robot joints, respectively. We have

$$\dot{x}_c = [J_{hc}(q) \quad J_{rc}(q)] \begin{bmatrix} \dot{q}_h \\ \dot{q}_r \end{bmatrix}. \quad (5)$$

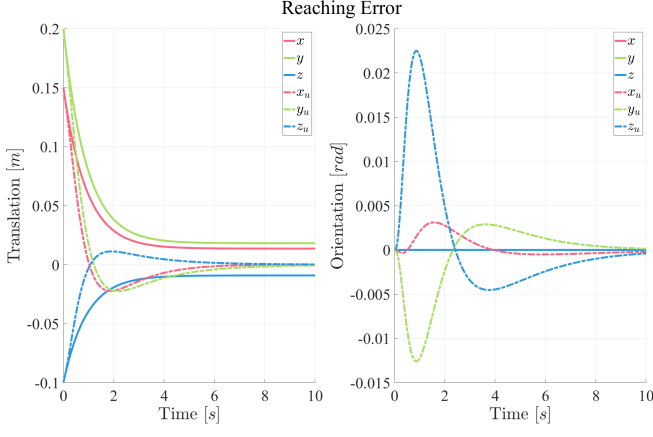


Fig. 2. Reaching error in a linear simulation: translation and orientation components of the reaching error e_e without (continuous line) and with (dashed line) prosthetic controller. $\Lambda_e = 1 I_6$ and $\Lambda_c = 0.1 I_6$. The reaching error $e_e(0)$ is initialized at $[0.15, 0.2, -0.1]$ for the translation component, and zero for the orientation.

In terms of reaching and compensation error dynamics, we write

$$\begin{bmatrix} \dot{e}_e \\ \dot{e}_c \end{bmatrix} = \begin{bmatrix} \dot{x}_e \\ \dot{x}_c \end{bmatrix} - \begin{bmatrix} J_{he}(q) & J_{re}(q) \\ J_{hc}(q) & J_{rc}(q) \end{bmatrix} \begin{bmatrix} \dot{q}_h \\ \dot{q}_r \end{bmatrix}. \quad (6)$$

Notice explicitly that the J_{rc} term can be used to model cases where the robotic system influences the body compensation variables, as e.g. when an active exoskeleton is included. Our goal in this paper is to design a controller for the robotic joints such that the prosthesis helps the user to reach their goal $x_e \rightarrow \bar{x}_e$, while allowing the compensatory motions to be reduced by bringing back $x_c \rightarrow \bar{x}_c$. In the following, we will assume that the relaxed configuration \bar{x}_c is constant. In the error coordinates, the goal is simply to stabilize both e_e and e_c in zero. To design the controller, we will assume that the configurations of both robot and human joints are measured in real time (via conventional encoders on the robot part, and motion capture systems for the human), so that x_c and x_e are known, and so is e_c . However, we cannot reasonably assume that \bar{e}_e is known, as the human intended goal \bar{x}_e is only known to the human, and not available for designing the feedback controller.

III. APPROACH

To illustrate the proposed solution to the problem presented in the previous section, we start from a simplified analysis of the system in proximity of the desired equilibrium $(e_e, e_c) = 0$. To model the relationship between the human motion and the reaching and compensation error, we assume a most simple linear proportional model, i.e. we assume that the human tends to move so as to reduce the reaching error target

$$\hat{J}_{he} \dot{q}_h = \Lambda_e e_e, \quad (7)$$

while at the same time trying to reduce compensation through

$$\hat{J}_{hc} \dot{q}_h = \Lambda_c e_c, \quad (8)$$

where Λ_e, Λ_c are generic diagonal (or, more generally, positive definite symmetric) square gain matrices. The matrices \hat{J}_{he}

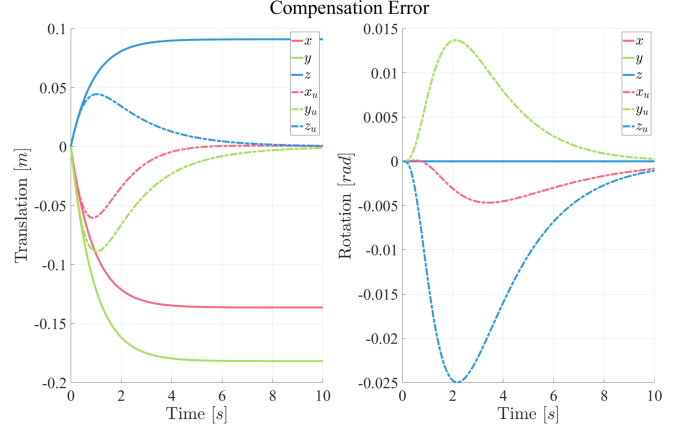


Fig. 3. Compensation error in a linear simulation: translation and orientation components of the compensation error e_c without (continuous line) and with (dashed line) prosthetic controller. $\Lambda_e = 1 I_6$ and $\Lambda_c = 0.1 I_6$. Initial conditions on the compensation error $e_c(0)$ are set to zero.

and \hat{J}_{hc} symbolically represent here the human internal model of the kinematic maps, i.e. how the subject expects her/his movements to be reflected in the hand and the compensatory movements, respectively. We will discuss the realism of these assumptions, and the choice of parameters, later. Of course, it will not be possible for the human joint velocities \dot{q}_h to satisfy both equations at the same time, so the system of (7) and (8) is inconsistent in general. It can be assumed that a solution for human joint velocities \dot{q}_h is chosen by subjects that weighs the reaching and compensation goals differently. This can be formalized as an optimization problem with cost

$$C_w(\dot{q}_h) = w \|\hat{J}_{he} \dot{q}_h - \Lambda_e e_e\|^2 + (1-w) \|\hat{J}_{hc} \dot{q}_h - \Lambda_c e_c\|^2 \quad (9)$$

for some $w \in [0, 1]$. For notational simplicity, define

$$\hat{J}_h = \begin{bmatrix} \hat{J}_{he} \\ \hat{J}_{hc} \end{bmatrix}, J_r = \begin{bmatrix} J_{re} \\ J_{rc} \end{bmatrix}, \Lambda = \begin{bmatrix} \Lambda_e & 0 \\ 0 & \Lambda_c \end{bmatrix},$$

and

$$\xi = \begin{bmatrix} e_e \\ e_c \end{bmatrix}, W = \begin{bmatrix} wI & 0 \\ 0 & (1-w)I \end{bmatrix}.$$

In this more compact notation, (7) and (8) are stacked as

$$\hat{J}_h \dot{q}_h = \Lambda \xi \quad (10)$$

while the index to be optimized in (9) can be rewritten as

$$C_w(\dot{q}_h) = \left(\hat{J}_h \dot{q}_h - \Lambda \xi \right)^T W \left(\hat{J}_h \dot{q}_h - \Lambda \xi \right).$$

It can be easily shown that, if the matrix $J_w := \hat{J}_h^T W \hat{J}_h$ is invertible, the optimal solution to (10) is

$$\hat{q}_h = J_w^{-1} \hat{J}_h^T W \Lambda \xi. \quad (11)$$

Notice that to have invertibility of J_w it is sufficient that \hat{J}_h has full column rank, i.e. that all human joints q_h considered in the model participate in controlling either the task or compensation frames. This can be assumed to happen, up

to possibly removing redundant joints from the human body model¹.

Substituting (11) in (6) we get

$$\dot{\xi} = \dot{\hat{x}} - J_h J_w^{-1} \hat{J}_h^T W \Lambda \xi - J_r \dot{q}_r. \quad (12)$$

This equation can be regarded as a dynamic system with state ξ , input $u = \dot{q}_r$, exogenous reference $r = \dot{\hat{x}} = \begin{bmatrix} \dot{\hat{x}}_e \\ \dot{\hat{x}}_c \end{bmatrix}$, and measurable output $y = e_c$, and rewritten as

$$\begin{cases} \dot{\xi}(t) = A\xi(t) + Bu(t) + r(t) \\ y(t) = C\xi(t) + Du(t) \end{cases}, \quad (13)$$

where

$$A = -J_h J_w^{-1} \hat{J}_h^T W \Lambda \quad B = -J_r, \quad (14)$$

$$C = \begin{bmatrix} 0 & I_6 \end{bmatrix}, \quad D = 0. \quad (15)$$

It should be noticed that, because the Jacobians are functions of the configurations q and so are the states, the system in (13) is nonlinear, with $A = A(\xi, t)$ and $B = B(\xi, t)$ in general. However, in a neighborhood of an equilibrium configuration with $\bar{\xi} = (\bar{q}_h, \bar{q}_r)$ and zero velocity ($\bar{u} = 0$), a linear approximation of system (6) is simply obtained by substituting the constant matrices $J_{he}(\bar{q})$, $J_{re}(\bar{q})$, $J_{hc}(\bar{q})$, and $J_{rc}(\bar{q})$ in A and B .

A. Control of Physically Connected Human–Robot Systems

We first consider here cases where the human and robot bodies are physically connected, such as in the first three rows of fig. 1. In these cases, we assume that internal kinematic maps \hat{J}_{he} and \hat{J}_{hc} are reasonably accurate, and can be identified with the actual Jacobians J_{he} and J_{hc} of the kinematic model presented in (6). These represent the Jacobians responsible for the reaching and compensation tasks, taking into account the contribution of the human joints. This assumption is justified with the ability of humans to include in their body schema devices and appendages, and to control them accurately in space, as mentioned before. Therefore, $\hat{J}_{he} \equiv J_{he}$, $\hat{J}_{hc} \equiv J_{hc}$ and $\hat{J}_h \equiv J_h$. In such a linearized system, the transition matrix A is a product of a projector matrix ($J_h J_h^\dagger$, where $J_h^\dagger = J_w^{-1} J_h^T W$) times a block diagonal matrix of human gains Λ , which is reasonable to assume to be positive definite. Hence, given the minus sign in A , system (13) is at least marginally stable in any ξ . This result corresponds to the observation that motions of humans with a passive prosthesis are stable, with some components of the error ξ going to zero, while others (notably, compensation errors) may only reach a non-null steady state if the prosthesis does not have enough DoFs.

It is at this point that the control of the robot or prosthesis intervenes to improve the situation, with the goal of helping the system reach the goal ($e_e = 0$) while canceling the compensation ($e_c = 0$) and restore a comfortable posture of the human body. To do so, one can design an output feedback

controller $u = u(y)$ (i.e., $\dot{q}_r = \dot{q}_r(e_c)$) in the form of a linear regulator with standard design methods. We hence proceed to estimate the reaching error e_e (which we assume to be known to the human, but not available to the controller) by exploiting the measured compensation error e_c , with the help of an asymptotic observer as

$$\begin{cases} \dot{\hat{e}} = A\hat{e}(t) + Bu(t) + L(\hat{y} - y(t)) \\ \hat{y}(t) = C\hat{e}(t). \end{cases} \quad (16)$$

By suitable choice of L , we can stabilize the observer dynamics, and thus obtain an estimate of the unknown intended target of human motion. We can then design a controller $u = -K\hat{e}$, thus obtaining an overall output-feedback stabilization that will eventually lead to $e_e \rightarrow 0$. More details on the choice of L and K will be given shortly.

Notice that complete reachability of all states may require enough dexterity of the robot or prosthesis, and full observability may need rich sensorization of compensation movements. If such properties are not warranted, however, the control designer's goal will be limited to place reachable and observable eigenvalues to a desirable location, while leaving others in their fixed, stable positions.

Results in fig. 2 report simulations obtained in Matlab/Simulink for the linearized system without and with the stabilizing controller for a prosthetic user with 7 robotic DoFs. It can be observed that the user initially reduces the reaching error at the expense of the compensation error (fig. 3). Indeed, the subject must perform compensatory motions to reach the desired end-effector pose x_e without being able to move the prosthetic arm. As soon as the observer for e_e reaches convergence, the robot controller kicks in and the prosthesis is actuated in the direction of the goal, so that also the compensation error is reduced to zero.

The observer-based control scheme presented above for the linearized model near an equilibrium can be applied to the general, nonlinear model (13) by an iterative relinearization scheme in the current working point, similar to what customarily done with Extended Kalman Filters (EKF). In other words, knowing that the joint configurations will vary at each time step t as $q_h(t)$, $q_r(t)$, the Jacobian matrices ($J_{he} = J_{he}(t)$, $J_{hc} = J_{hc}(t)$, $J_{re} = J_{re}(t)$, $J_{rc} = J_{rc}(t)$) and the state matrices $A = A(t)$ and $B = B(t)$ are recomputed and used for computing the controller and estimator gains.

Accordingly, we apply a straightforward Linear Quadratic Gaussian (LQG) regulator design by iteratively recomputing the K and L matrices along the executed motions. Using the standard EKF procedure, the Kalman estimator gain is computed as

$$L = PC^T R_{cov}^{-1},$$

with P the estimated state covariance matrix and R_{cov} the covariance matrix of the observation noise. The estimated state covariance matrix is updated as

$$\dot{P} = AP + PA^T - LCP + Q_{cov},$$

¹Equivalently, the solution can be expeditely obtained by solving $\hat{J}_h^T W \hat{J}_h \dot{q}_h = \hat{J}_h^T W \Lambda \xi$ as $\hat{q}_h = J_w^\dagger \hat{J}_h^T W \Lambda \xi$.

with Q_{cov} the covariance of the process noise. For the control part, we recurrently compute the controller gain K so as to minimize the cost function

$$\int_{t=0}^{\infty} (e^T Q e + u^T R u + 2e^T S u) dt,$$

where Q is the state-cost weight matrix, R the input-cost weight matrix, and S is the mixed input-state weight matrix (normally set to zero). Fast algorithms to solve such equations and compute the K and L matrices in real time are readily available as open-source code.

Although there is no formal proof of stability for the iterative relinearization technique above described, widespread practice shows that the scheme works well for mildly nonlinear systems, such as the human-robot system at hand. Simulations and experimental results reported below confirmed this.

B. Control of Physically Disconnected Human–Robot Systems

Somehow surprisingly, the proposed method can also be adapted to the pilot-avatar scenario depicted in the last row of fig. 1, where a user acts in a remote environment through a physically disconnected avatar.

Indeed, because of the physical robot-user disconnection, in (6) it holds $J_{he} = 0$. Should also the human model in (7) include $\hat{J}_{he} = J_{he} = 0$, the operator could only try to solve the compensatory task, and not act on the robot at all. However, this contrasts with common experience in observing pilots in virtual reality and in tele-operation systems [19], and even in commercial videogames. Indeed human operators often move their bodies and try (sometimes even very hard) to move the end-effector toward a task *as if* they were the avatar to which the end-effector belongs. In other words, the pilot immerses into the remote environment through the perspective of the robot avatar, usually by viewing the environment through the robot's eyes (e.g. via a head mounted display (HMD) system). This phenomenon could be regarded as a generalized version of the *rubber hand* effect, a rather well studied illusion in the psychological literature (see e.g. [20]).

Based on this observation, we postulate that the human internal model \hat{J}_{he} is not equal to the real $J_{he} = 0$ in this case. Rather, the operator uses for \hat{J}_{he} the kinematic map of the avatar's arm *as if* the arm itself was attached to the operator's body. Given that when using avatars the egocentric frame of reference is translated in the avatar's head, this assumption is tantamount to having an internal model of the kinematic map from the avatar's head to the avatar's hand, imagined as controlled by the pilot's own body replacing the avatar's. Notice explicitly that, here as well as in the section above, the internal model \hat{J}_{he} considers the artificial arm frozen in the present configuration.

IV. NUMERIC ANALYSIS

This section provides a numerical validation of the proposed control algorithm, considering two scenarios commonly encountered in rehabilitation robotics. The first scenario involves an upper-limb prosthetic user, while the second features the application of the Alter-Ego avatar robot as an assistive device.

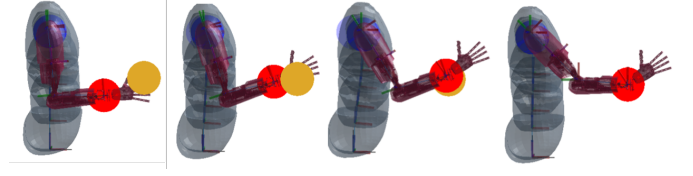


Fig. 4. Simulation 1: sequence of frames for $x_0 = [0, -0.5, 0]$ rad for the orientation component and $x_0 = [0.2, -0.1, 0.1]$ m for the translation component.

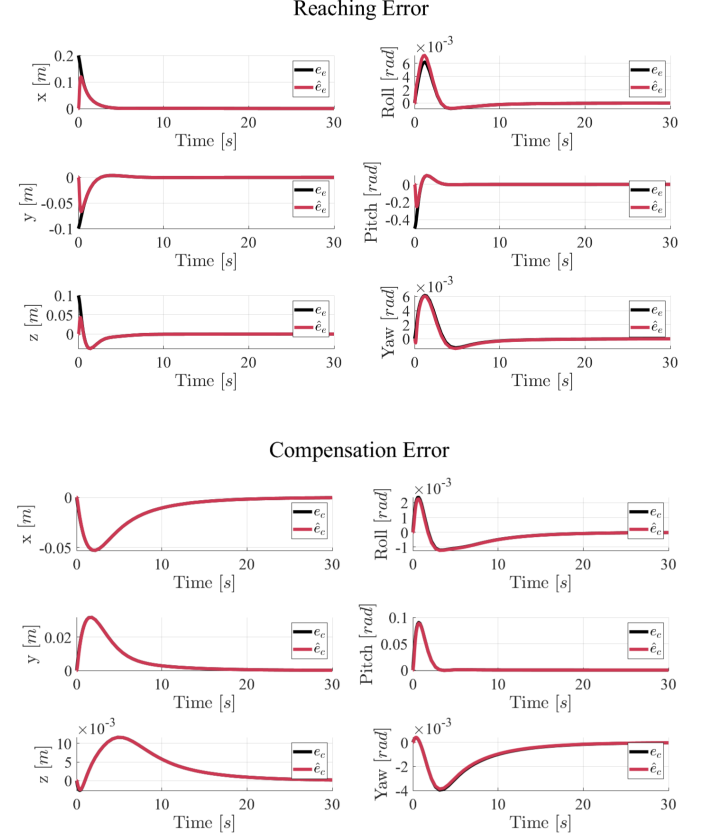


Fig. 5. Simulation 1: translational and rotational components of reaching and compensation errors. Actual values are depicted in black, their EKF estimates in red.

Both cases are later replicated in the experimental section. While in the experimental setup compensatory motion inputs will be directly taken from the human subjects, in numerical simulations human motions are generated by our assumed model (11). Thus, this section aims to illustrate that these assumptions lead to results consistent with expectations, i.e. that a predefined target pose, \bar{x}_e , is reached, while robot joints move so as to allow the compensatory motions to be ultimately relaxed. All simulations are carried out using Matlab/Simulink.

A. Simulations of Physically Connected Human-Robot System

Our first simulations focus on the control of a transcapular prosthesis with seven degrees of freedom. Notice that in current prosthetic practice, no known system exists which can simultaneously control such a complex system. In our simulated prosthesis, both the shoulder and wrist have three DoFs, while the elbow has one. The compensation frame

is placed at the scapula, just before the attachment of the prosthesis. The human behavior is modeled according to (11). Following (16), at each time step we calculate the observer and gain matrices L and K by solving the LQG design procedure at the instantaneous system configuration.

Two simulation runs are shown for illustration, as reported in fig. 4 and fig. 6, respectively. Human body parts are represented in gray, while artificial parts are in purple. In both cases, the user starts from a neutral, “home” configuration and has to reach a desired final pose with the hand, with both a desired position and orientation. The desired position is farther than the home configuration in fig. 4, and closer in fig. 6. In both cases, our models generate first a compensatory motion of the comensatory frame in the direction of the target, triggering the prosthetic joints (purple). On the last step, the prosthetic hand frame (red dot) has reached the desired target frame (yellow dot), while the human body has returned to the relaxed initial posture.

Fig. 5 and 7 report the translational and rotational components of errors, corresponding to simulation runs of fig. 4 and fig. 6, respectively. The plots report both actual (black) and estimated (red) values of reaching and compensation errors, and show good convergence of all values to zero.

B. Simulation of Physically Disconnected Human-Robot System

The last simulation focuses on the pilot-avatar scenario, where the user aims for the avatar to reach a predefined end-effector pose. In this case, the pilot assumes the perspective of the robot by viewing the environment through the robot’s eyes (e.g. by wearing a HMD displaying the robot’s camera outputs).

As described in a previous section, we consider in this scenario the Jacobian matrix \hat{J}_{he} to represent the map from the human reference frame (identified with the avatar’s own) to the end-effector of the artificial arm.

The derivation of the human controller and the controller follows as above, where however the system matrix A for this case is

$$A = -J_h \bar{J}_w^\dagger \hat{J}_h W \Lambda, \quad (17)$$

$$\text{with } J_h = \begin{bmatrix} 0 \\ J_{hc} \end{bmatrix} \text{ and } \hat{J}_h = \begin{bmatrix} \hat{J}_{he} \\ J_{hc} \end{bmatrix}.$$

For this study, we employed the Alter-Ego robot [21], a two-wheeled auto-balancing humanoid avatar. The robot has a mobile base for translation and rotation, along with two robotic arms, each with 5 DoFs, attached to the main robotic body. Considering its kinematics, we designated the matrix J_{re} as the Jacobian matrix of the entire robotic chain from the global frame (fixed to the ground) to the right end effector, thus being influenced by the joints of the wheels and the right arm. The robotic base is described by the x and y coordinates of the center of its base, and by the orientation angle θ around the vertical axis z . The base motions are modeled as a unicycle, with the translation and rotation velocities as inputs.

The simulation was implemented in Matlab/Simulink by specifying a desired reaching pose for the robot’s right end-effector. The human motion is simulated by the model (11),

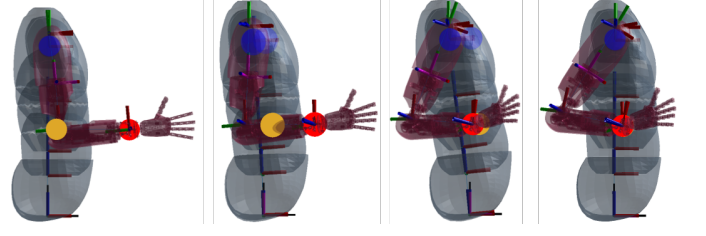


Fig. 6. Simulation 2: sequence of frames for $x_0 = [-0.2, 0, -0.8]$ rad for the orientation component and $x_0 = [-0.25, -0.1, 0]$ m for the translation component.

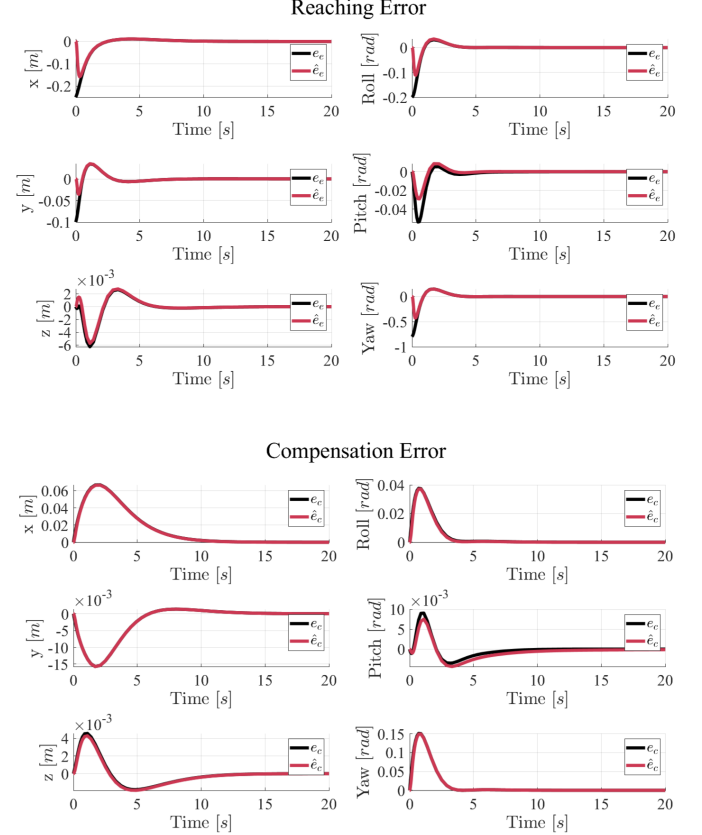


Fig. 7. Simulation 2: translational and rotational components of reaching and compensation errors. Actual values are depicted in black, their EKF estimates in red.

while the EKF and controller are computed based on (17). The sequence of frames for this simulation is depicted in fig. 8 and fig. 9. Convergence of both reaching and compensation errors, and estimates thereof, are reported in fig. 10.

C. Stability Margins

It should be noticed that the regulator design uses estimates of the unknown human gain matrices Λ_e and Λ_c . These matrices are subject-dependent, and can be estimated by means of experiments conducted directly on each subject (see below in the experimental section). It is to be expected in any case that even their customized estimate will not exactly reflect reality (including here the likely fact that the linear relationships assumed in (7) and (8) may not be valid except for a neighborhood of the equilibrium). In reality, then, we will have to deal with a perturbed system model, whereby the

computation of the regulator matrices uses an estimate of the system dynamics.

Establishing the limits for the estimation error within which the regulator still guarantees stability of the system is a problem in robust control which is not studied here. We note however that, even if such bounds could be established mathematically, their application to the case at hand would not be not trivial without a thorough psychophysical analysis. To provide a glimpse into the robustness properties of the method, however, we report in fig. 11 results of a few simulations for the linearized system of a prosthetic user with 7 robotic DoFs, where we assume the true human control parameters to be normalized at $\Lambda_e = \Lambda_c = 1 I_6$, and their estimates $\hat{\Lambda}_e$ and $\hat{\Lambda}_c$ to vary in the range $[10^{-2} I_6, 10^2 I_6]$. For each simulation test, the behavior of reaching and compensation errors is simulated. In the plot, we highlight in green the values of $\frac{\hat{\Lambda}_e}{\Lambda_e}$ and $\frac{\hat{\Lambda}_c}{\Lambda_c}$, for which a stable behavior is maintained.

V. EXPERIMENTS AND RESULTS

We validate our approach through two experimental scenarios designed to assess the algorithm's performance across several robotic degrees of freedom. We include a video in the attachment of this study showing both simulated and experimental implementations. We implement the two experiments in the Robot Operating System (ROS) Noetic framework and use MVN XSens 2021.2 as Inertial Measurement Units (IMUs) to track the user's upper-body compensatory motions. In both cases, the user performs compensatory motions, which are read as human joint angles and processed by the central ROS node. We define the user-dependent kinematics for computing the Jacobian matrices according to the Unified Robot Description Format (URDF) conventions. The final output consists of the prosthetic joint positions. The following subsections provide a detailed description of the principal outcomes obtained in the experimental sessions.

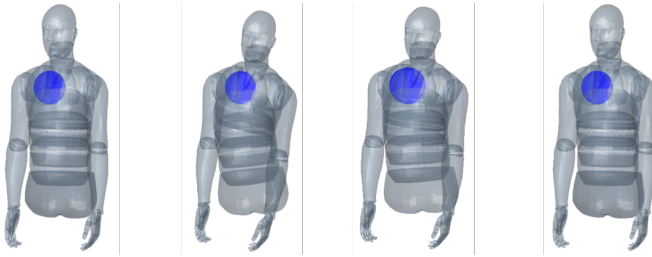


Fig. 8. Simulation 3: compensatory behavior of the user. The starting conditions for the reaching error are set equal to $x_0 = [0, -0.5, 0]^T \text{ rad}$, for the orientation and $x_0 = [1, 0, 0.1]^T \text{ m}$ for the translation. The blue dot placed on user's shoulder identifies the compensation frame.

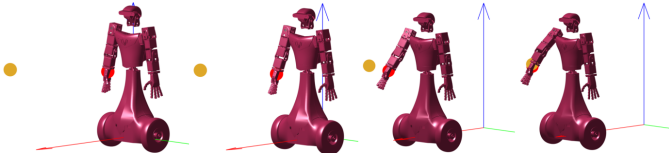


Fig. 9. Simulation 3: reaching motion of the avatar. The robot end effector (red dot) reaches the desired pose (yellow dot) through coordinated control of base and arm.

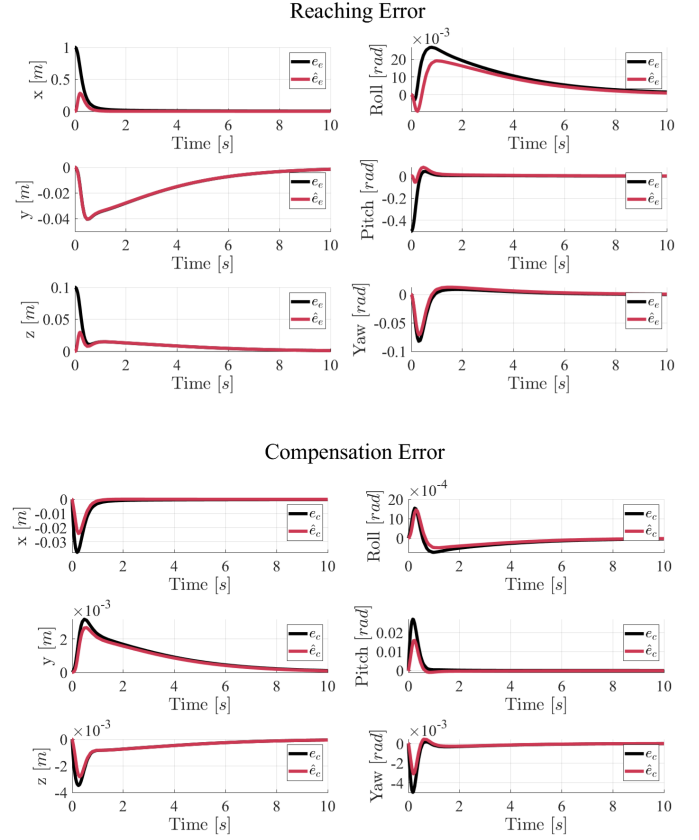


Fig. 10. Simulation 3: translational and rotational components of reaching and compensation errors. Actual values are depicted in black, their EKF estimates in red.

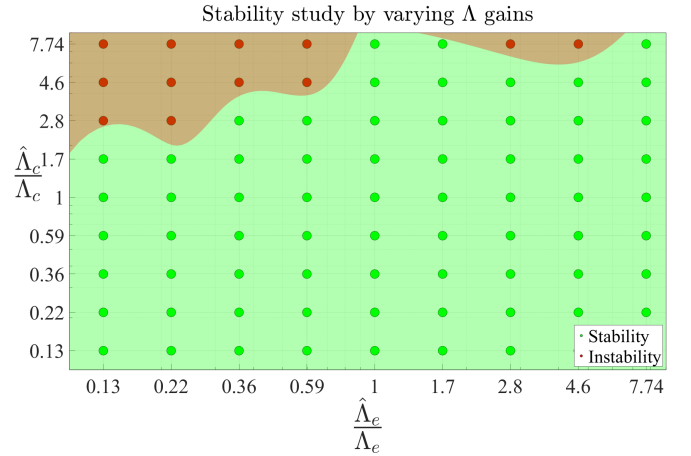


Fig. 11. Stability of the system as the ratios of estimate and real human model parameters, $\frac{\hat{\Lambda}_e}{\Lambda_e}$ and $\frac{\hat{\Lambda}_c}{\Lambda_c}$, are varied. Green dots represent relative errors for which stability is maintained, while in red dots instability occurs.

A. Experiments with a Virtual Upper-Limb Prosthesis

In the first set of experiments, we validate the proposed controller by testing it with a real user of a virtual prosthesis. To do so, we build a kinematically accurate digital twin of the subject, and replicate motions captured from the subject in the twin in real time. Virtual prostheses, with 3, 4 and 7 DoFs respectively, are used in different experiments. The

virtual prostheses are virtually donned to different sections of the intact subject's arm. The amputation level is known to the experimenter and is used to set the human and prosthesis models in the controller.

The user wears IMU sensors on their upper body and looks at their virtual twin on a screen. A picture of the setup used for this experiment is reported in fig. 12. The subject is instructed to reach the desired object, depicted as a red sphere in the virtual environment by moving the attachment section of the virtual prosthesis in their own body. The subject is instructed not to move the parts of their real arm corresponding to the prosthesis in use. Even if instructions are not followed, however, motions of these parts are filtered and discarded as they are irrelevant to the controller.

Compensatory motions of the user are tracked and mapped onto the virtual twin. The algorithm interprets compensatory motions to directly control the robotic joints of the virtual prosthesis.

Remark. The choice of where the compensatory frame should be placed requires some consideration. In cases where the artificial limb is a prosthesis of a distal part of the upper

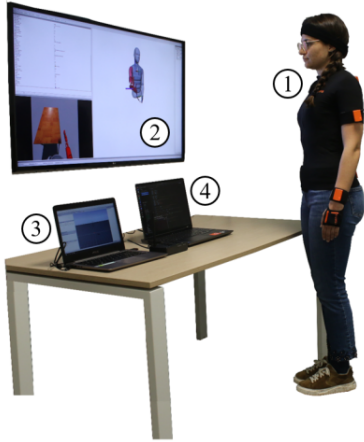


Fig. 12. Experimental setup. 1: user tracked via XSens sensors. 2: Monitor for visualization of the virtual twin. 3: PC for XSens tracking. 4: PC with controller.

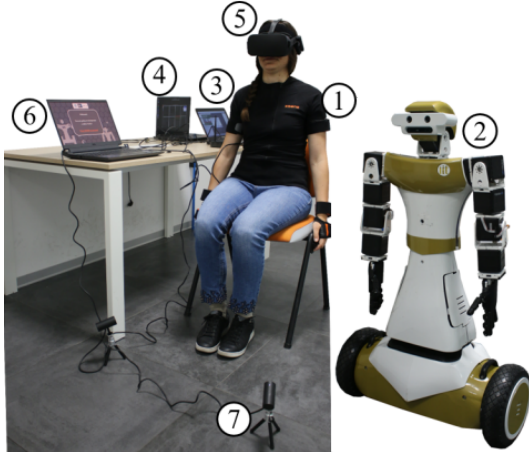


Fig. 13. Experimental setup. 1: user tracked via XSens sensors. 2: Alter-Ego robot. 3: PC for XSens tracking. 4: PC with controller. 5: Oculus Rift. 6: PC for Oculus software. 7: Towers for Oculus calibration.

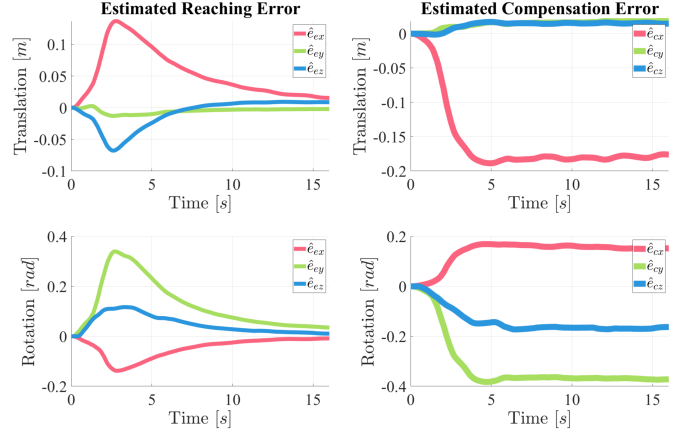


Fig. 14. 7 DoFs user with the prosthetic controller turned off: estimation of the reaching error \hat{e}_e (left) and of the compensation error \hat{e}_c for the case of the prosthetic controller turned off.

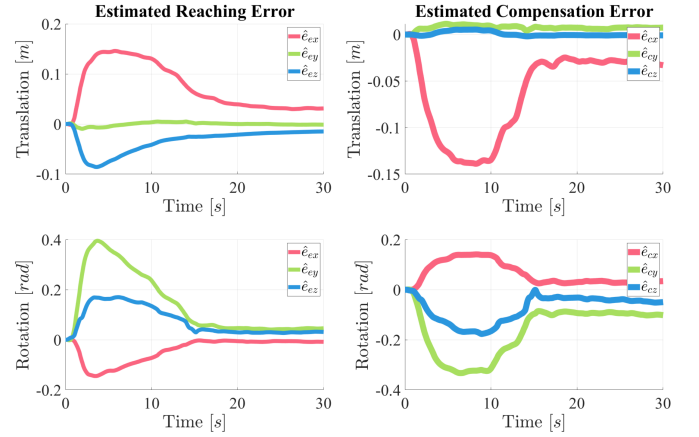


Fig. 15. 7 DoFs user with the prosthetic controller turned on: estimation of the reaching error \hat{e}_e (left) and of the compensation error \hat{e}_c for the case of the prosthetic controller turned on.

limb, for instance, one could ask whether the most distal section of the body available for IMU instrumentation should be used as compensatory frame. However, if the compensatory frame is placed distally, e.g. on the forearm stump for a transradial amputation, then the feedback policy of bringing $e_c \rightarrow 0$ would imply that the user eventually brings their forearm to “home” (rest) configuration. Thus, the functional parts of the arm would not participate in the reaching task, which would have to be solved by the prosthesis alone. By placing the compensation frame at the user's shoulder instead, the final configuration will see the partly human, partly artificial upper limb joints both participate in reaching, while the shoulder and torso will eventually return to rest pose. We use this solution in our experiments below. However, it should also be emphasized that in other scenarios than the prosthetic arm case, and with different users, the choice could be different - as e.g. with robot avatars for patients with very limited residual mobility and/or strength, where instead compensation frames could be placed at the most distal available body parts.

In a first set of experiments, we disabled the robot prosthesis controller (i.e., we set $\dot{q}_r = 0$), and only focused on the model of the human compensatory behaviour. Through a series of

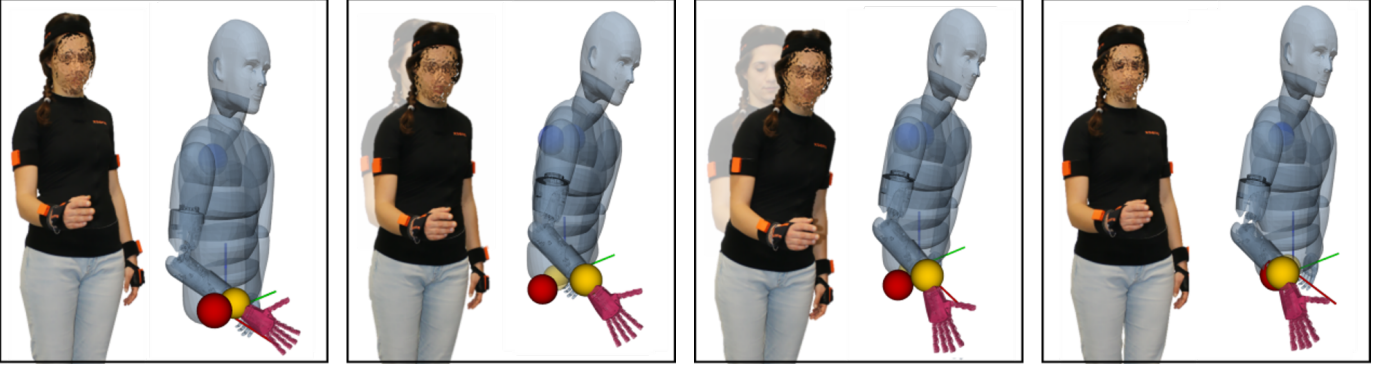


Fig. 16. Scenario 1: sequence of frames for the transradial amputation case, with 3 prosthetic DoFs.

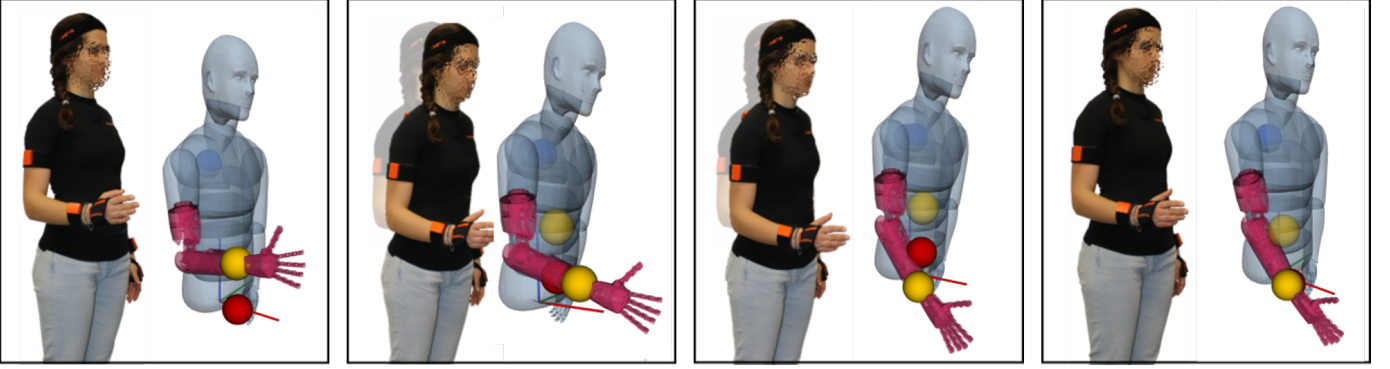


Fig. 17. Scenario 2: sequence of frames for the transhumeral amputation case, with 4 prosthetic DoFs.

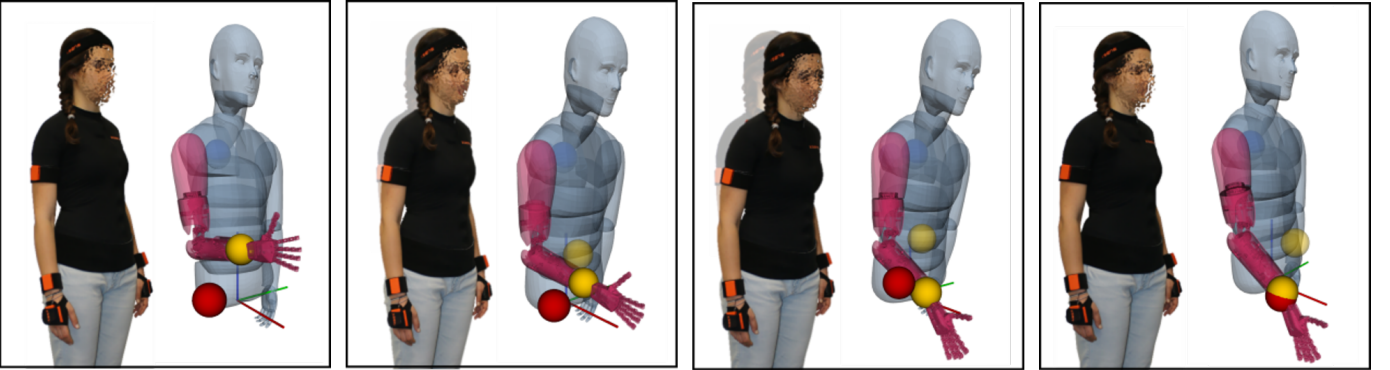


Fig. 18. Scenario 3: sequence of frames for the shoulder disarticulation case, with 7 prosthetic DoFs.

repeated experiments and an empirical optimization, the parameters of the subject's model were estimated to $\Lambda_c = 0.1 I_6$, $\Lambda_e = 2 I_6$.

With the controller turned off and a 7 DoF arm fixed in the initial configuration, large compensatory motions are expected to be needed to reach the target. Results depicted in fig. 14 highlight how the reaching error estimate (depicted on the left side) converge to zero. As expected, the reaching target is obtained at the expenses of the compensation error (on the right side), which remains large. Notice that, although we do measure compensation errors, we report here their estimates, which practically amounts to a filtered versions of the IMU sensor outputs via the Kalman filter used in our scheme.

In a subsequent experiment, the same target is approached

with the robot controller active, so that the prosthetic joints assist the user in reaching the desired end-effector pose and reduce the compensatory shoulder displacement, as depicted in fig. 15. It can be observed that compensation movements are similar at the beginning with the previous case with the controller turned off, but are quickly reduced by the prosthesis controller intervention. Convergence of the reaching error estimates is shown to have similar dynamics as in the previous case. A number of experiments of this type was used to tune the controller parameters as $P(0) = \text{diag} [10, 10, 10, 10, 10, 10, 10, 0.05, 0.05, 0.05, 0.05, 0.05]$, $R_{cov} = 0.01 I_6$, $Q_{cov} = I_{12}$, $R = I_7$, and $S = 0$. Finally, $Q = \text{diag} [0, 0, 0, 0, 0, 0, 10, 10, 10, 0.1, 0.1, 0.1]$ was chosen, reflecting the different scaling of translational and rotation

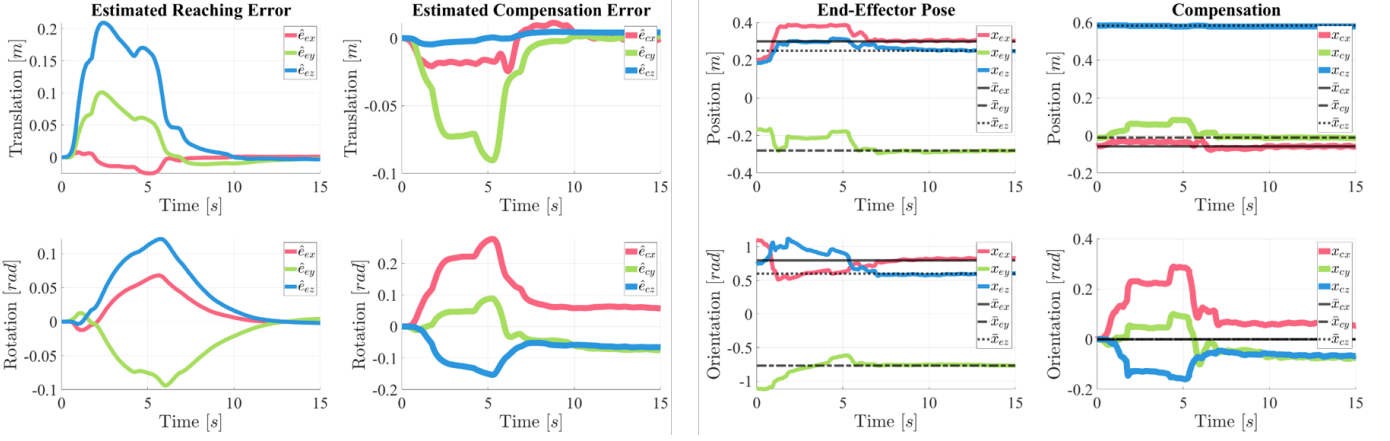


Fig. 19. Scenario 1: estimation of the reaching and compensation errors and actual reaching and compensation frames for the transradial amputation case.

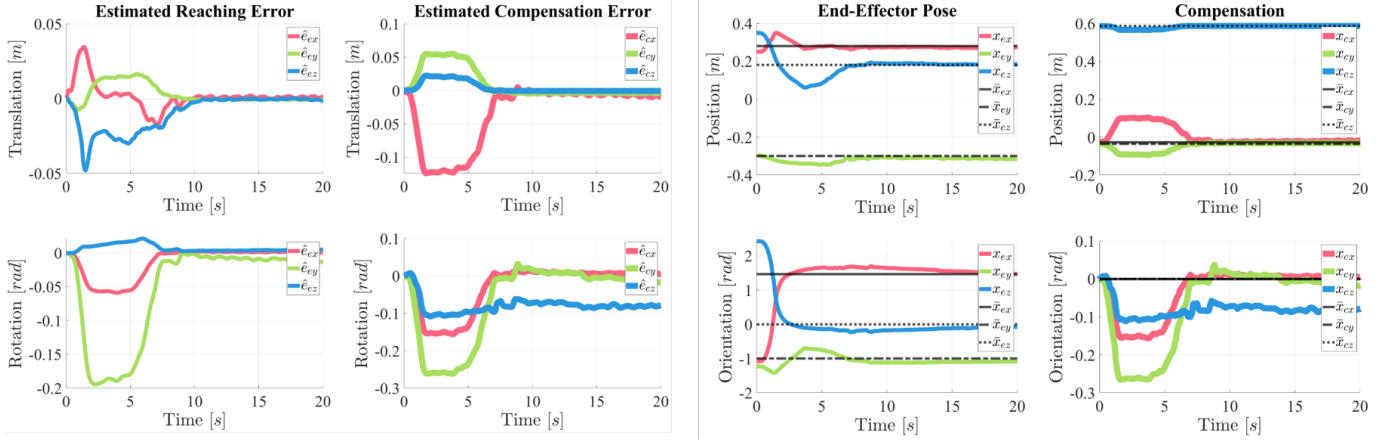


Fig. 20. Scenario 2: estimation of the reaching and compensation errors and actual reaching and compensation frames for the transhumeral amputation case.

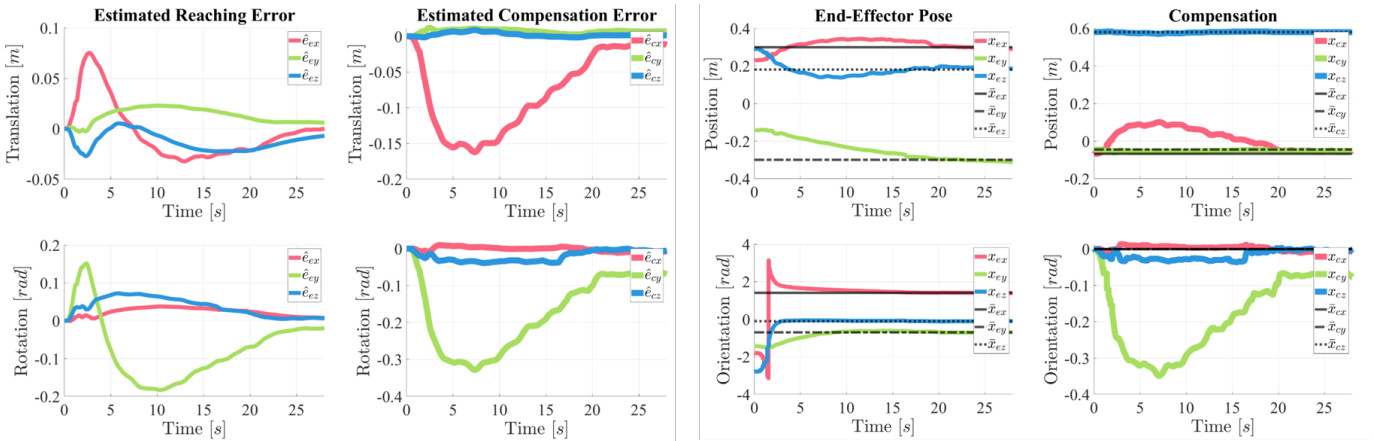


Fig. 21. Scenario 3: estimation of the reaching and compensation errors and actual reaching and compensation frames for the shoulder disarticulation case.

components (measured in meters and radians, respectively).

With values obtained by calibration and tuning, we performed more experiments for three different prostheses corresponding to different amputation levels. The first case involves a transradial amputation requiring control over 3 DoFs (fig. 16), a transhumeral case follows with 4 DoFs (fig. 17), and the final scenario refers to a shoulder disarticulation with

7 DoFs (fig. 18). In figs. 16, 17, and 18, user's compensatory motions are visualized by showing the reference configuration in transparency, and the prosthetic motions in the virtual environment. The blue dot represents the compensatory frame, the yellow dot is at the actual reaching frame x_e , and the red dot is at the desired frame \bar{x}_e . Blue and yellow dots in transparency depict the compensatory and reaching frame

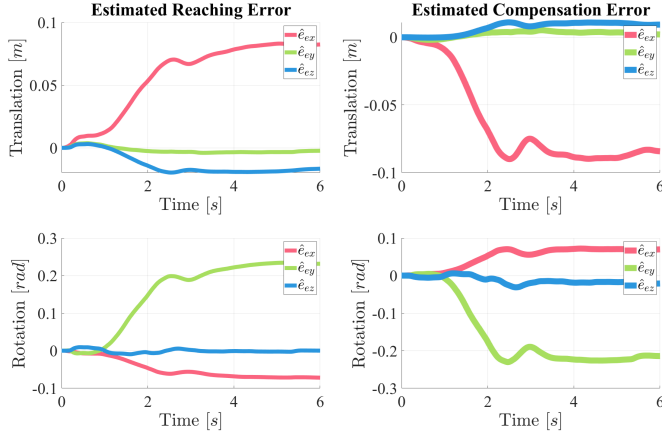


Fig. 22. Pilot-avatar case with the robotic controller turned off: estimation of the reaching error \hat{e}_e (left) and of the compensation error \hat{e}_c , for the case of the robotic controller turned off.

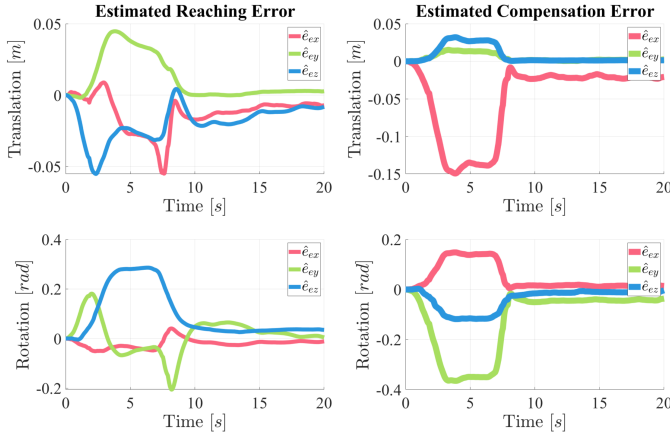


Fig. 23. Pilot-avatar case with the robotic controller turned on: estimation of the reaching error \hat{e}_e (left) and of the compensation error \hat{e}_c , for the case of the robotic controller turned on.

respectively at the starting configuration. As it can be seen, as soon as the user starts to produce compensatory motions (which are directly mapped into the virtual twin's shoulder motions), the controller starts generating commands for the prosthesis. Once the subject is satisfied with the target pose achieved by the robotic hand, they go back to their starting posture, stopping the prosthesis motion $\dot{q}_r = 0$.

Figs. 19, 20, and 21 present plots corresponding to the 3DoF, 4DoF, and 7DoF prosthetic user scenarios, respectively. For each case, plots on the two left-most columns display convergence of the estimated reaching error and compensation error, respectively, to zero. Plots on the right side show instead the actual pose reached by the prosthesis hand, in comparison with the desired final pose, and the compensation frame pose, compared to the target relaxed pose. As shown, in all cases the robotic hand successfully reaches the desired target, even though the controller is unaware of its pose. Once the target is reached, the compensation is progressively relaxed.

B. Experiment with a Whole-Body Prosthesis

In the second experiment, we validate the algorithm for the two-wheeled humanoid robotic avatar Alter-Ego [21]. Robotic joints to be controlled here include not only those belonging to the arm (5 joints for the right arm) but also the wheeled base. The base is modelled by the kinematics of a unicycle, as described in Section IV. In this setup, the robot functions as a sort of “whole-body” prosthesis of the person, who perceives the robot avatar as an artificial extension of their own body. The user views the environment through Alter-Ego's eyes using an Oculus Rift as shown in fig. 13. This setup allows the user and the robot to be in different physical locations. The user's compensatory frame motions, tracked via IMU sensors, trigger the controller. We placed the compensatory frame at the user's right shoulder. The key difference from the previous experiment is that, in this case, the reaching task is entirely handled by the robot using both wheels, shoulder and arms to reach the user's intended hand posture, without that being known.

We place the reaching frame on Alter-Ego's right palm, and - similarly as in the previous experiment described in fig. 14 - first verify the correct functioning of the observer while keeping the robot still, i.e. $\dot{q}_r = 0$. As shown in fig. 22, the compensation error does not approach zero. Different from fig. 14, neither the estimated reaching error converges to zero in this case, because the compensation does not produce any motion of the hand, being physically disconnected.

When the controller is turned on, both reaching and compensation errors converge to zero, as depicted in fig. 23. As in the previous case, these preliminary experiments led to an empirical optimization of the controller parameters, setting $P(0) = \text{diag}[10, 10, 10, 10, 10, 10, 10, 0.05, 0.05, 0.05, 0.05, 0.05, 0.05]$, $R_{cov} = 0.01 I_6$, $Q_{cov} = I_{12}$, $R = I_7$, and $S = 0$. and $Q = \text{diag}[0, 0, 0, 0, 0, 0, 100, 100, 100, 0.1, 0.1, 0.1]$.

In a first set of experiments, we have a human user virtually connected to a digital twin of the Alter-Ego robot in a virtual environment. The user's compensatory motions are tracked by XSens sensors.

Before executing a complete reaching task, we assess the functionality of the robot control for individual user motions to observe how they translate into the robot's actions. As depicted in fig. 24, we illustrate the compensatory motions of the user along the positive and negative directions of the x and y axes of the global frame (box on the bottom left corner). The x axis is represented in red, and the y axis in green. The compensation frame is consistently placed on the user's right shoulder, and the end-effector frame on the robot's right palm. The user starts from an upright posture (in transparency) and starts movements towards the direction of the object to be grasped. For each user motion, we observe the corresponding motion of Alter-Ego's right arm from the home configuration (in transparency) towards the final configuration. The yellow arrow highlights the direction of the robot's base motion. Under each pilot-avatar motion, we present the corresponding estimation of the reaching and compensation errors, for both translation and rotation components.

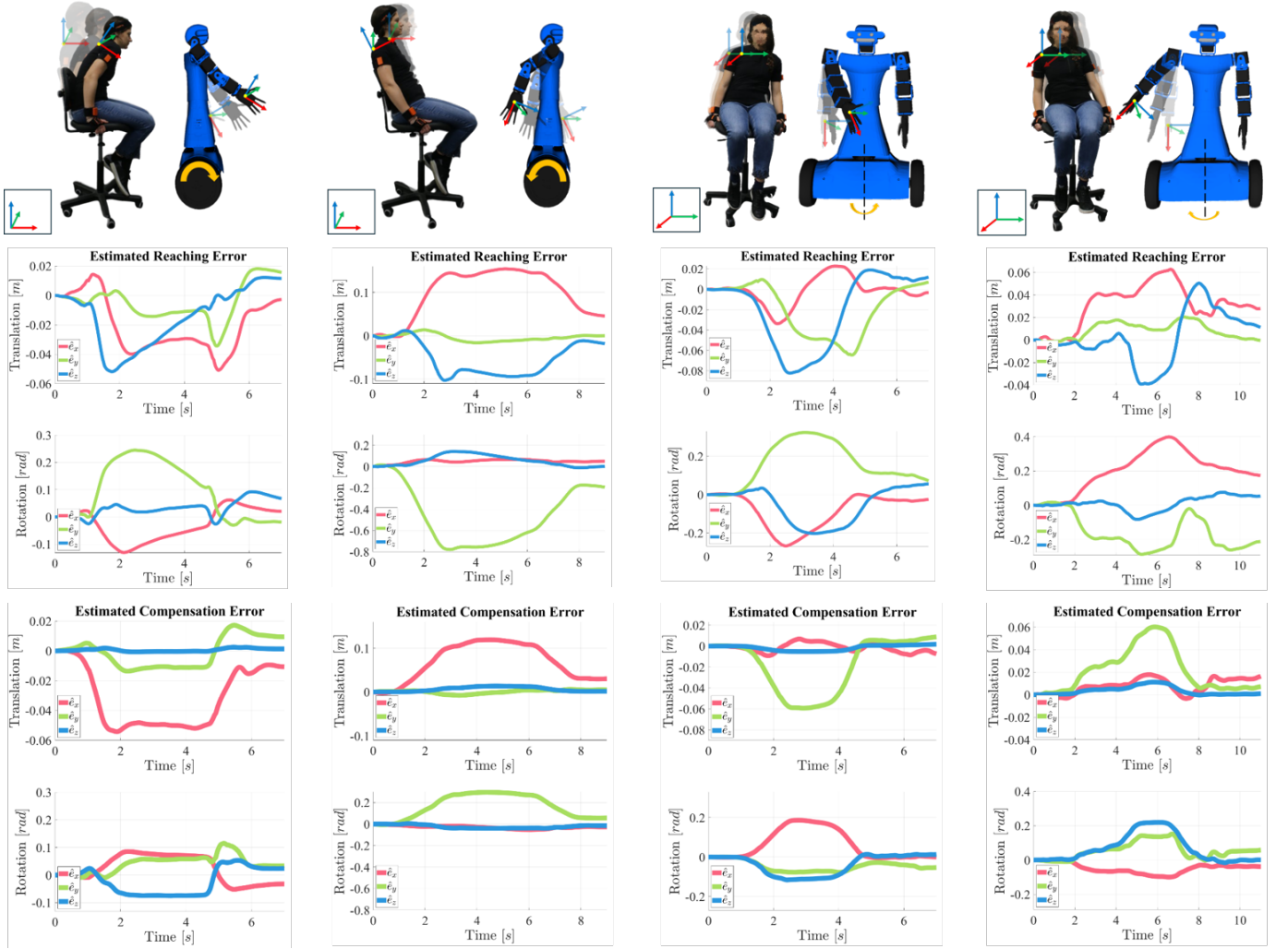


Fig. 24. Individual user motions to drive Alter-Ego along positive and negative directions of x axis and positive and negative directions of y axis of the global frame, displayed in the box on the bottom left corner. Both user's and robot's old frames are depicted in transparency. Below each case, the corresponding plots for both reaching and compensation errors are reported.

After using the first experiment to identify the human model and choose the controller parameters, the system functionality is tested on the more complex task of reaching for a red peg placed on a table far from the robot initial position. The peg is placed far enough that the use of the arm only is not sufficient, and the wheeled base must also translate and rotate to reach for the peg. The user looks at the virtual scene through a camera placed on Alter-Ego's eyes, whose image is reproduced in a real display mounted on the head of the human user. User motions are tracked by the XSens suite sensors, and used to drive the robot controller as described above.

Fig. 25 shows six consecutive frames of the execution of this task in a virtual reality environment. User's compensatory motions, shown in the first row of fig. 25, are also reproduced in a virtual twin (second row). The twin is reported here for visualization purposes only, while it is not used in the control, nor is it seen by the user. The third row shows the virtual robot avatar reaching for the peg, while the bottom row provides the views from the camera positioned on the robot's head and reproduced in the head-mounted display.

Fig. 26 shows the estimated reaching errors \hat{e}_e and the estimated compensation errors \hat{e}_c for this task. As observed, the errors converge to zero by the end of the task. In fig. 27, we plot the actual pose of the end effector and of the compensation frame (in colors) versus the desired ones (in black).

Following the calibration phase and verification in simulation, we report here results of implementation of the reaching task on a physical version of Alter Ego. In fig. 30, we present a sequence of six frames illustrating the user motion (top row) and robot motion (middle row) as the robot hand reaches the desired goal, i.e. a water bottle on the table. The bottom row shows the camera view from the robot's perspective, as displayed to the user.

The estimated reaching and compensation errors are reported in fig. 28. In fig. 29 we present the physical hand pose x_e compared to the desired \bar{x}_e , as well as the actual compensation frame x_c versus the target \bar{x}_c . As it can be observed, the method drives the hand to reach for the distant target using both wheels and arm movements to accommodate for both position and orientation, using only the user's shoulder

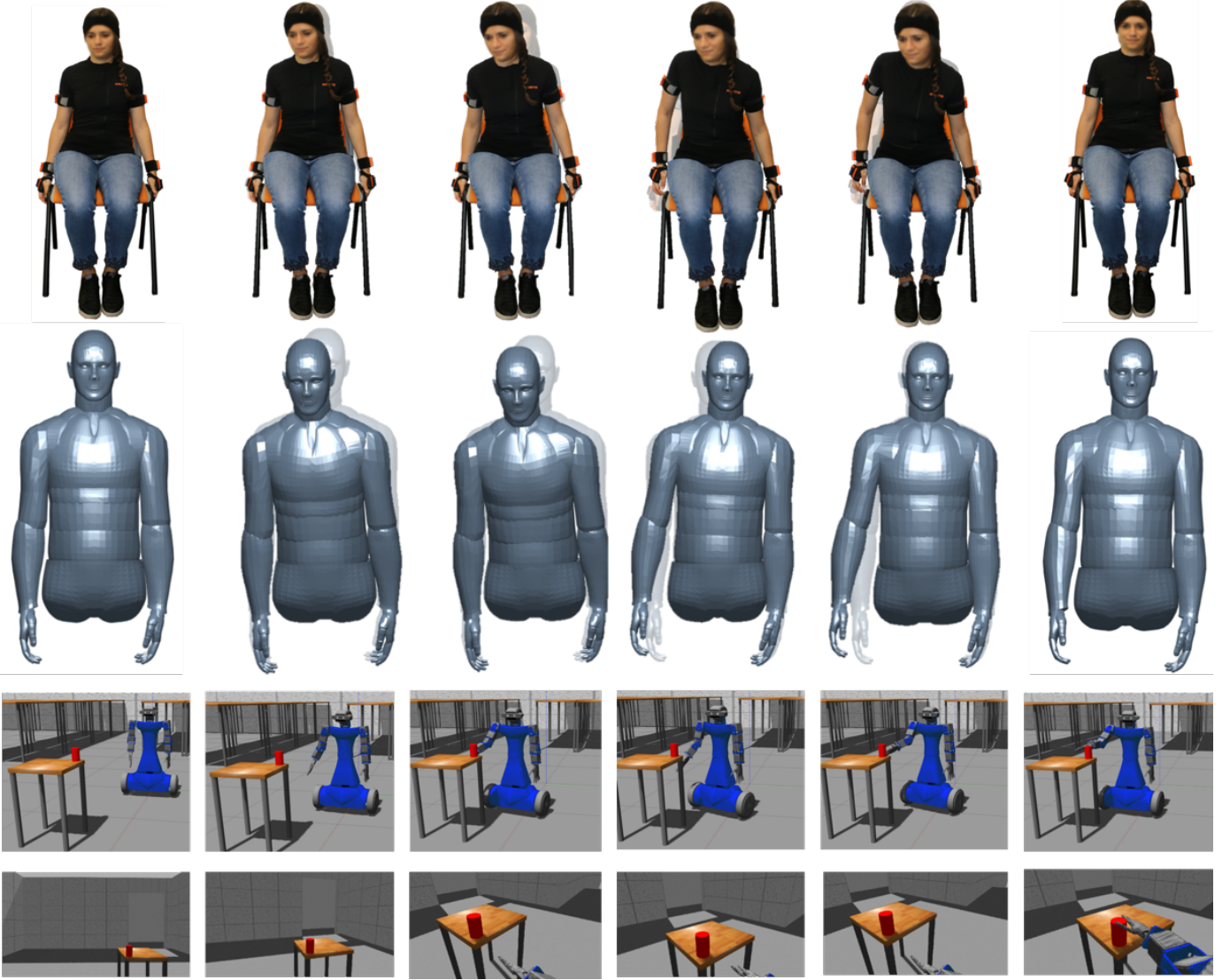


Fig. 25. Six frames of the reaching task with virtual model of Alter-Ego. We report the user’s motions, tracked via XSens, the corresponding user’s virtual twin, Alter-Ego’s motion in virtual environment, and the view from the camera placed on Alter-Ego’s eyes.

der position as input, eventually allowing the user to go back to a relaxed posture.

VI. DISCUSSION

Our research moved from previous work [14] showing how users of simple prosthetic devices tend to make up for missing DoFs by performing so-called compensatory motions with the functional parts of their body, and how these motions can be used to drive the active prosthetic limbs and reduce compensation.

In this paper we extend this intuition to the control of more complex systems where humans and robots take physical part. We outline a theoretical framework encompassing a dynamical system where both human and robot dynamics are integrated, design its control, and validate it via both virtual experiments, where human motions tracked via IMU sensors command virtual prostheses with 3, 4 and 7 DoFs, respectively.

The generality of the approach allowed us to further extend this algorithm to a broader range of applications, basically

including all combinations of human and robot kinematics, as depicted in fig. 1. In our experiments we focused on the control of a robot avatar, regarded as a “whole-body prosthesis”, using only few compensatory motions of the user.

The functionality of the approach was demonstrated through experiments, where the measured and estimated compensation errors largely coincide, and the estimate of the (unmeasurable) reaching error is reduced to zero. The controller generates robotic commands based on user motions, and, as soon as the user returns to their relaxed posture, the robotic joints stop moving.

Our results demonstrate that estimating the reaching error based on user’s compensatory motions is indeed possible, and that this makes it possible to guide robotic devices to achieve the target the user aims at, without that being ever explicit. Our approach allows the user to focus on the desired goal, without the need to directly control each joint independently, as done in conventional prosthetic control. The user’s interaction with robotic devices is thus substantially simplified, enhancing

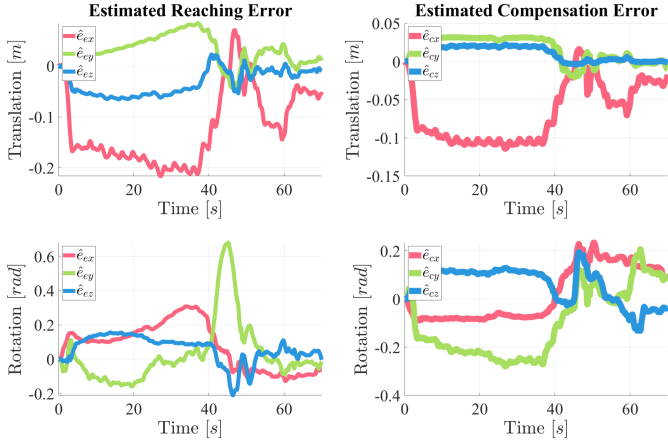


Fig. 26. Estimated reaching and compensation errors for the VR reaching task.

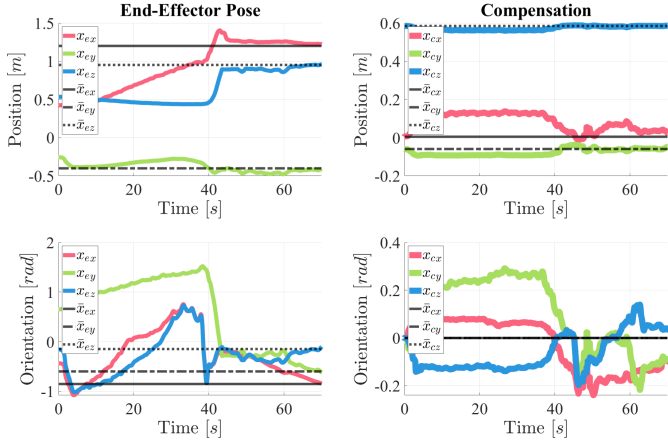


Fig. 27. Actual pose of the end effector, x_e , and of the compensation frame, x_c , vs the desired ones, \bar{x}_e and \bar{x}_c , in the VR reaching task.

usability and efficiency.

Given the user's crucial role in triggering the control, the framework's effectiveness heavily depends on the user's residual motion abilities. This implies that the control system should be tailored on the user. Tuning weighting matrices in the controller affects the behaviour of the human-robot integrated system, which can be used to match certain task requirements. For instance, favoring the use of wheel motions over arm joints can enhance performance for specific applications where the robot should navigate the robot in a large free space before reaching the final target.

Another crucial point is the choice of the compensatory frame. In our experiments we placed this frame on the user's right shoulder. However, further studies could explore alternative positions, depending on the specific residual motions the user controls with ease, and on the robotic system to be controlled. This flexibility in the compensatory frame's placement could optimize the control strategy, tailoring it more closely to the individual user's capabilities and the requirements of different tasks.

Possible applications of the methods described here are to assist people with disabilities that limit their motions, such as those with neurological disorders. Preliminary tests (not described here) showed that a potential issue in this case are

involuntary reflex motions these individuals might experience. Implementing an algorithm for motion discrimination can significantly help in this context. The implementation would distinguish between intentional movements and involuntary reflexes, ensuring that only purposeful motions trigger the robotic commands. Additionally, integrating a deadband zone around the user's target posture can facilitate controller deactivation, particularly when significant residual motions are present. This deadband zone can also help in discriminating voluntary motions from the involuntary ones of the shoulders, associated from example with breathing [22]. Further research into incorporating kinematics studies in the control process could improve robotic movements, enhancing overall system performance.

Lastly, it is worth to point out that the hardware platforms used to demonstrate our method in this paper are mere examples, and other developments could generalize and/or simplify the apparatuses - e.g., using visual-based motion capture could replace IMU sensors and minimize hardware, to make the system more practical and user-friendly.

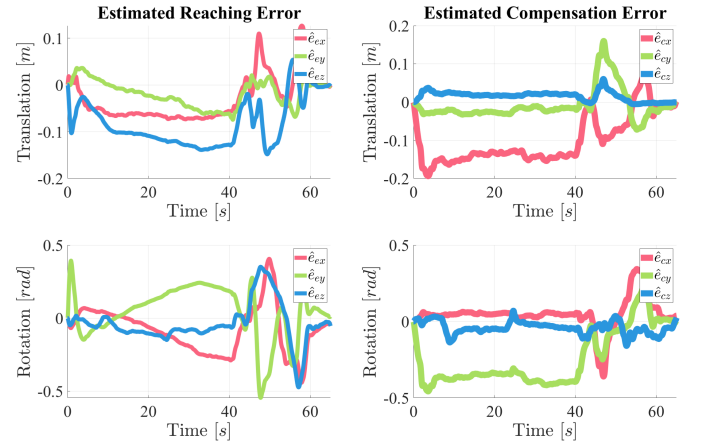


Fig. 28. Estimated reaching and compensation errors for the real robot reaching task.

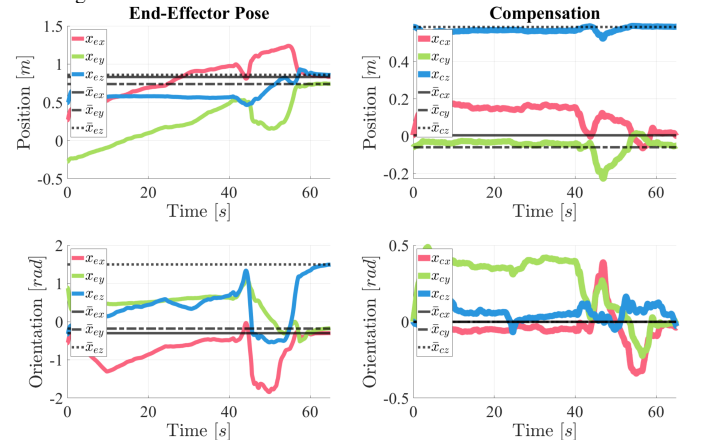


Fig. 29. Actual pose of the end effector, x_e , and of the compensation frame, x_c , vs the desired ones, \bar{x}_e and \bar{x}_c in the real robot reaching task.

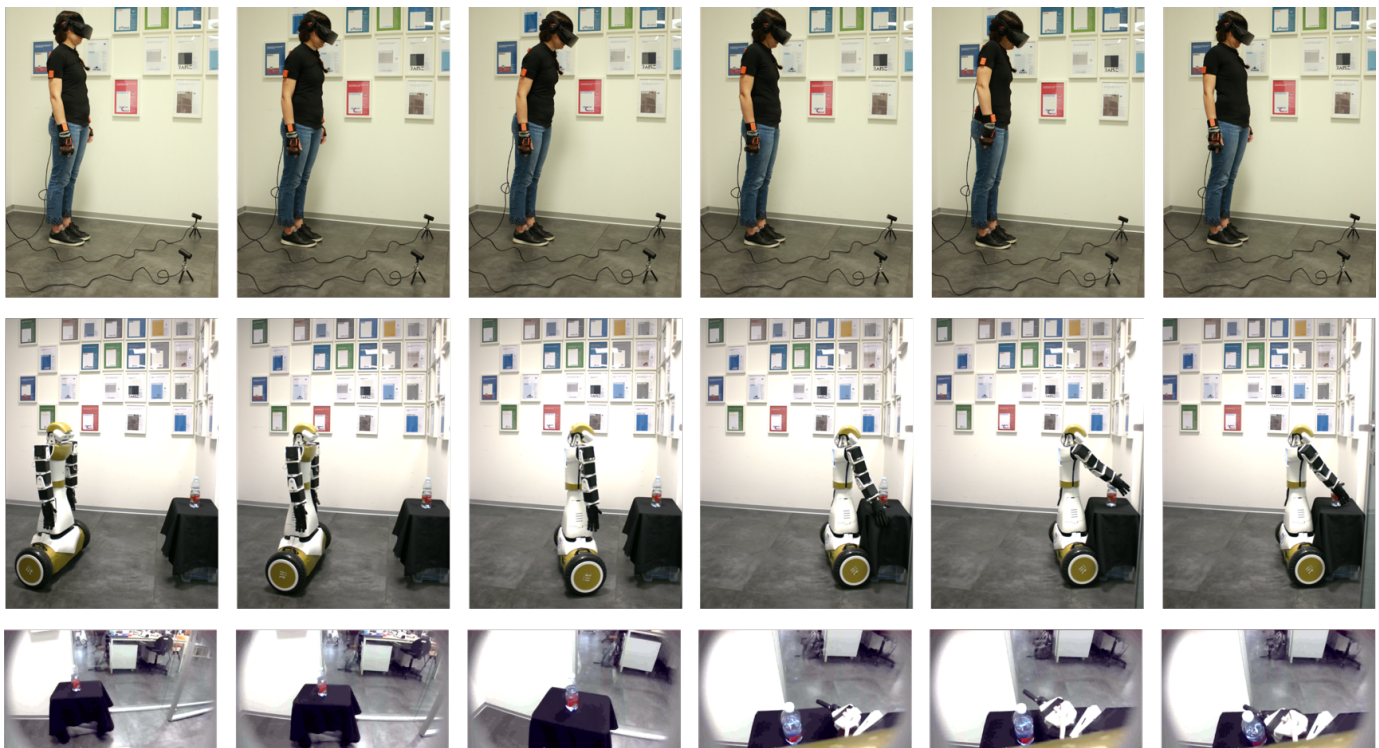


Fig. 30. Six frames of the reaching task with the physical Alter-Ego robot. We report the user's motions (top), tracked via XSens, Alter-Ego's motion in real environment (middle), and the view from the camera placed on Alter-Ego's eyes (bottom).

VII. CONCLUSION

This paper demonstrates the potential of a general control framework for systems integrating human and robotic bodies of different shapes and DoFs. Simulations and experiments illustrate its applicability across different types of robots. A main characteristic of looking at the human and robot as parts of the same system is that redundancy in the overall systems makes it possible to reach and maintain a desired hand target while minimizing the user's effort and discomfort. Possible applications are various, including e.g. ergonomics of teleoperation. Another important possible application is to assistance and rehabilitation.

To enhance the controller's robustness, however, further tests are necessary. These will involve conducting user case studies to evaluate the usability and feasibility of this framework in various applications. Among the planned tests, we aim to work with prosthetic users to directly assess the control's functionality and compare it with traditional prosthetic control techniques. Ongoing studies will also focus on assistance to patients with limited motion abilities, including multi-subjects studies to evaluate the usability of the Alter-Ego robot by individuals with spinal cord injuries or patients with amyotrophic lateral sclerosis (ALS).

ACKNOWLEDGMENTS

This work was supported in part by the European Research Council Synergy Grant Natural BionicS (NBS) project (Grant Agreement No. 810346).

This work was carried out within the framework of the project "RAISE - Robotics and AI for Socio-economic

Empowerment" and has been supported by European Union - NextGenerationEU.

Funded by the European Union - NextGenerationEU. However, the views and opinions expressed are those of the authors alone and do not necessarily reflect those of the European Union or the European Commission. Neither the European Union nor the European Commission can be held responsible for them.

This work was supported by the Italian Ministry of Research, under the complementary actions to the NRRP "Fit4MedRob - Fit for Medical Robotics" Grant (# PNC0000007).

Thanks to Giovanni Rosato, Manuel Barbarossa and Eleonora Sguerri for the technical support.

REFERENCES

- [1] D. Gopinath, S. Jain, and B. D. Argall, "Human-in-the-loop optimization of shared autonomy in assistive robotics," *IEEE Robotics and Automation Letters*, vol. 2, no. 1, pp. 247–254, 2017.
- [2] S. Jain, A. Farshchian, A. Broad, F. Abdollahi, F. Mussa-Ivaldi, and B. Argall, "Assistive robotic manipulation through shared autonomy and a body-machine interface," in *IEEE International Conference on Rehabilitation Robotics*, vol. 2015. IEEE, 08 2015.
- [3] D. Edakkattil Gopinath, M. Nejati, and B. Argall, "Customized handling of unintended interface operation in assistive robots," in *IEEE International Conference on Robotics and Automation (ICRA)*, Xi'an, China, 07 2020, pp. 10 406–10 412.
- [4] J. M. Lee, T. Gebrekristos, D. D. Santis, M. Nejati-Javaremi, D. Gopinath, B. Parikh, F. A. Mussa-Ivaldi, and B. D. Argall, "Learning to control complex robots using high-dimensional interfaces: Preliminary insights," 2021.
- [5] L. Hochberg, D. Bacher, B. Jarosiewicz, N. Masse, J. Simeral, J. Vogel, S. Haddadin, J. Liu, S. Cash, P. van der Smagt, and J. Donoghue, "Reach and grasp by people with tetraplegia using a neurally controlled robotic arm," *Nature*, vol. 485, pp. 372–5, 05 2012.

- [6] A. Sanna, F. Lamberti, G. Paravati, and F. Manuri, "A kinect-based natural interface for quadrotor control," *Entertainment Computing*, vol. 4, p. 179–186, 08 2013.
- [7] A. Stoica, F. Salvioli, and C. Flowers, "Remote control of quadrotor teams, using hand gestures," in *9th ACM/IEEE International Conference on Human-Robot Interaction*, 03 2014, pp. 296–297.
- [8] D. Praticchizzo, M. Pozzi, T. Lisini, M. Malvezzi, I. Hussain, S. Rossi, and G. Salvietti, "Human augmentation by wearable supernumerary robotic limbs: Review and perspectives," *Progress in Biomedical Engineering*, vol. 3, p. 042005, 10 2021.
- [9] E. Lamon, F. Fusaro, P. Balatti, W. Kim, and A. Ajoudani, "A visuo-haptic guidance interface for the mobile collaborative robotic assistant (moca)," in *IEEE/RSJ International Conference on Intelligent Robots and Systems*, 10 2020.
- [10] S. Farr, N. Catena, S. Martinez-Alvarez, and F. Soldado, "Peromelia – congenital transverse deficiency of the upper limb: A literature review and current prosthetic treatment," *Journal of Children's Orthopaedics*, vol. 12, pp. 1–8, 10 2018.
- [11] A. Roche, H. Rehbaum, D. Farina, and O. Aszmann, "Prosthetic myoelectric control strategies: A clinical perspective," *Current Surgery Reports*, vol. 2, 03 2014.
- [12] S. Carey, M. Highsmith, M. Maitland, and R. Dubey, "Compensatory movements of transradial prosthesis users during common tasks," *Clinical biomechanics (Bristol, Avon)*, vol. 23, pp. 1128–35, 08 2008.
- [13] M. Maimeri, C. Della Santina, C. Piazza, M. Rossi, M. G. Catalano, and G. Grioli, "Design and assessment of control maps for multi-channel semg-driven prostheses and supernumerary limbs," *Frontiers in Neurorobotics*, vol. 13, 2019. [Online]. Available: <https://www.frontiersin.org/articles/10.3389/fnbot.2019.00026>
- [14] M. Legrand, N. Jarrasse, F. Richer, and G. Morel, "A closed-loop and ergonomic control for prosthetic wrist rotation," in *IEEE International Conference on Robotics and Automation*, 05 2020, pp. 2763–2769.
- [15] M. Merad, N. Jarrasse, E. Montalivet, M. Legrand, E. Mastinu, M. Ortiz-Catalan, A. Touillet, N. Martinet, J. Paysant, and A. Roby-Brami, "Assessment of an automatic prosthetic elbow control strategy using residual limb motion for transhumeral amputated individuals with socket or osseointegrated prostheses," *IEEE Transactions on Medical Robotics and Bionics*, vol. PP, pp. 1–1, 01 2020.
- [16] M. Legrand, N. Jarrasse, C. Marchand, F. Richer, A. Touillet, N. Martinet, J. Paysant, and G. Morel, *Controlling Upper-Limb Prostheses with Body Compensations*. Springer, Cham, 01 2022, pp. 101–106.
- [17] M. Feder, G. Grioli, M. G. Catalano, and A. Bicchi, "Implicit upper-limb prosthesis control from compensatory body motions," in *Experimental Robotics*, M. H. Ang Jr and O. Khatib, Eds. Cham: Springer Nature Switzerland, 2024, pp. 535–544.
- [18] M. Merleau-Ponty, *Phenomenology of Perception*. D. Landes, Trans.; 1st ed, Routledge., 2010.
- [19] J. Betancourt, B. Wojtkowski, P. Castillo, and I. Thouvenin, "Exocentric control scheme for robot applications: An immersive virtual reality approach," *IEEE Transactions on Visualization and Computer Graphics*, vol. 29, no. 7, pp. 3392–3404, 2023.
- [20] M. Flögel, P. Beckerle, and O. Christ, "P244: Rubber hand and rubber foot illusion: a comparison and perspective in rehabilitation," *Clinical Neurophysiology*, vol. Volume 125, Supplement 1, p. S113, 06 2014.
- [21] G. Zambella, G. Lentini, M. Garabini, G. Grioli, M. Catalano, A. Palleschi, L. Pallottino, A. Bicchi, A. Settini, and D. Caporale, "Dynamic whole-body control of unstable wheeled humanoid robots," *IEEE Robotics and Automation Letters*, vol. PP, pp. 1–1, 07 2019.
- [22] A. Farshchiansadegh, F. Abdollahi, D. Chen, M.-H. Lee, J. Pedersen, C. Pierella, E. J. Roth, I. S. Gonzalez, E. B. Thorp, and F. A. Mussa-Ivaldi, "A body machine interface based on inertial sensors," in *2014 36th Annual International Conference of the IEEE Engineering in Medicine and Biology Society*, 2014, pp. 6120–6124.